

Machinable  $\alpha$ -SiAlON/BN CompositesRoman Shuba<sup>†</sup> and I-Wei Chen

Department of Materials Science and Engineering, University of Pennsylvania, Philadelphia, Pennsylvania 19104-6272

Dense machinable  $\alpha$ -SiAlON/BN composites were fabricated by hot-pressing using turbostratic boron nitride (tBN) obtained from nitridation of melamine diborate. The tBN was added to the starting powders, or introduced as a coating that formed *in situ* on  $\alpha$ -Si<sub>3</sub>N<sub>4</sub> carrier powders during nitridation, and was subsequently converted to hexagonal boron nitride (hBN) during hot pressing by solution reprecipitation. These composites maintain high strength at 1000°C and their strength/hardness are much higher than similar composites prepared using commercial hBN powder, which yielded a coarser microstructure. Good machinability was achieved despite a flat *R* curve.

## I. Introduction

MONOLITHIC Si<sub>3</sub>N<sub>4</sub>/SiAlON ceramics have excellent mechanical properties but poor machinability, which increases the fabrication costs. As a remedy, several  $\beta$ -Si<sub>3</sub>N<sub>4</sub>/BN “nanocomposites” have been reported that combine machinability and excellent mechanical properties.<sup>1–4</sup> To achieve this goal, it is imperative to maintain a highly homogeneous dispersion of fine BN particles. Such dispersion proves difficult for conventional powder mixing; in addition, the presence of highly refractory BN sometimes retards sintering. To circumvent these problems, *in situ* reaction (forming BN phase *in situ* during synthesis) is commonly used in fabricating “nanocomposites.”<sup>5–9</sup> Such work has not been reported for  $\alpha$ -SiAlON, which is the subject of the present study.

In the *in situ* forming approach for  $\beta$ -Si<sub>3</sub>N<sub>4</sub>/BN “nanocomposites,” a BN precursor, typically in the form of a mixture of boric oxide/acid and organic reducing agent (urea, melamine), is first introduced into the starting powders. After pyrolysis turbostratic BN (tBN) forms, intimately mixed with Si<sub>3</sub>N<sub>4</sub> and oxide powders. During subsequent sintering or hot pressing, tBN is converted into the thermodynamically stable hexagonal BN (hBN), which is responsible for improved machinability. This approach was taken by Kusunose *et al.* and Oku *et al.*, for example.<sup>1–4,10</sup> In their work, reaction of boric acid and urea in hydrogen gas at 1100°C, followed by annealing in nitrogen gas at 1500°C, was used to prepare tBN. The process, however, requires excess urea and a small gas overpressure in order to prevent the loss of urea (melting point = 133°C), making it difficult to control stoichiometry. These requirements were also reported by Yamamoto,<sup>11</sup> who described a method to obtain tBN by heating urea and boric acid in a ratio of more than 2:1 in a pressure vessel at 950°C. The poor stoichiometry control resulted in a BN product that was typically oxygen rich<sup>12</sup>; moreover, formation of hard agglomerates in a urea-based route requires prolonged milling, contributing to partial oxidation of nitride constituents. Such powders are unsuitable for fabricating  $\alpha$ -SiAlON composites because, in our experience, an oxygen-rich

composition shifts the phase assemblage from single-phase  $\alpha$ -SiAlON to two-phase  $\alpha$ -SiAlON/ $\beta$ -Si<sub>3</sub>N<sub>4</sub>.

The objective of this work is to prepare nanosized BN precursor using a stoichiometric melamine borate salt process,<sup>13–15</sup> and to use this precursor to fabricate  $\alpha$ -SiAlON/BN composites. The size effect of BN particles on microstructure development and mechanical properties of the composites will also be examined.

## II. Experimental Procedure

The nominal composition of  $\alpha$ -SiAlON/BN composites was Y<sub>0.5</sub>Si<sub>9.3</sub>Al<sub>2.7</sub>O<sub>1.2</sub>N<sub>14.8</sub> ( $m = 1.5$ ,  $n = 1.2$ , or Y1512) with  $x$  vol% BN ( $x = 0$ –20), designated as  $\alpha$ -SiAlON/ $x$ BN or simply  $x$ BN composite (see Table I). As a sintering aid, 2 wt% of La<sub>2</sub>O<sub>3</sub>, which does not enter the crystal lattice of  $\alpha$ -SiAlON, was added. The starting powders for  $\alpha$ -SiAlON were  $\alpha$ -Si<sub>3</sub>N<sub>4</sub> (SN-E10, UBE Industries, Ube, Japan), AlN (Type F, Tokuyama Soda Co., Burlingame, CA), Y<sub>2</sub>O<sub>3</sub> (99.995%, APS 25–50 nm, Alfa-Johnson Matthew Co., Ward Hill, MA), Al<sub>2</sub>O<sub>3</sub> (AKP50, Sumitomo Chemical America, NY), and La<sub>2</sub>O<sub>3</sub> (99.995%, APS 80 nm, Inframat Advanced Materials, Farmington, CT). Source chemicals for BN were H<sub>3</sub>BO<sub>3</sub> (99.5%, Acros Organics, Morris Planes, NJ) and melamine C<sub>3</sub>N<sub>6</sub>H<sub>6</sub> (99%, Acros Organics, Morris Planes, NJ). Commercial hexagonal BN (99.5%, Alfa-Johnson Matthew Co.) with a plate-like morphology (3–5  $\mu$ m diameter) was also used to fabricate reference composites for comparison. The oxygen content in  $\alpha$ -Si<sub>3</sub>N<sub>4</sub> (1.26 wt%) and AlN (0.82 wt%) was taken into account in the formulation. Seed crystals of Y1512 in the amount of 1% were also added in all cases to control the microstructure. The procedure for obtaining seeds reported elsewhere<sup>16–17</sup> was followed with the exception of using molten KOH, instead of a HNO<sub>3</sub>+HF mixture, as a washing agent. This was done to prevent fluoride contamination that is harmful to the high-temperature properties.

Preparation of composites is schematically depicted in Fig. 1. Melamine (72 g) was dissolved in boiling distilled water (2.5 l) and a solution of H<sub>3</sub>BO<sub>3</sub> (90 g, dissolved in 200 mL of water) was added to it during stirring. The mixture solution was cooled to room temperature to obtain melamine diborate (C<sub>3</sub>N<sub>6</sub>H<sub>6</sub>·2H<sub>3</sub>BO<sub>3</sub>) salt precipitate. This salt was washed with water to remove unreacted boric acid and dried in an oven at

Table I. Summary of SiAlON/BN Composites Described in the Text

% BN	Source of BN	Precursor pyrolysis temperature (°C) and gas composition
20	Si <sub>3</sub> N <sub>4</sub> coated with BN	900 (NH <sub>3</sub> )
20	Si <sub>3</sub> N <sub>4</sub> coated with BN	1500 (NH <sub>3</sub> ) + 1700 (N <sub>2</sub> )
0, 5, 10, 20	tBN	900 (NH <sub>3</sub> )
20	tBN	1500 (NH <sub>3</sub> ) + 1700 (N <sub>2</sub> )
20	hBN	No pyrolysis

BN, boron nitride; tBN, turbostratic boron nitride; hBN, hexagonal boron nitride.

T. Ohji—contributing editor

Manuscript No. 21079. Received October 16, 2005; approved February 19, 2006.

This research was supported by the U.S. Air Force Office of Scientific Research, Grant No. F49620-01-1-0150 and National Science Foundation, Grant No. DMR05-20020.

<sup>†</sup>Author to whom correspondence should be addressed. e-mail: roman@shuba.name

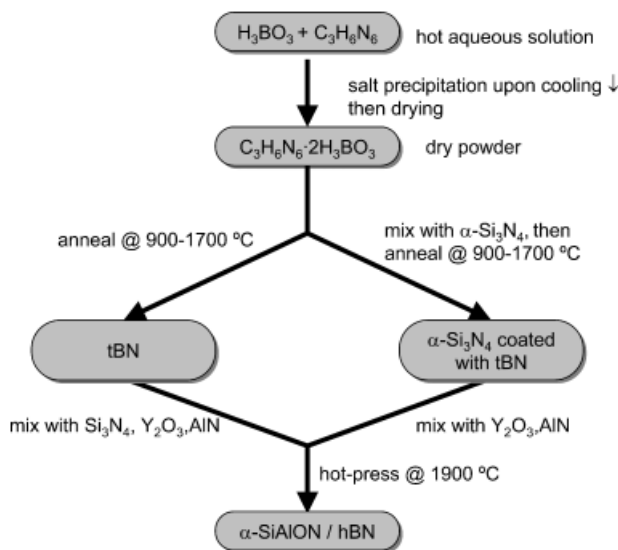


Fig. 1. Flowchart of composite fabrication, where tBN stands for turbostratic boron nitride and hBN for hexagonal boron nitride.

70°C for 24 h. It was next pyrolyzed in an alumina tube by heating, under flowing ammonia gas, at 1°C/min to 900°C, then held for 20 h, resulting in tBN. (As ammonia massively dissociated into nitrogen and hydrogen during pyrolysis, precautions were taken against the ignition of hydrogen). To obtain a tBN product that might be more stable, the pyrolysis temperature was also raised to 1500°C, held for 20 h, followed by annealing at 1700°C in a graphite furnace for 2 h in nitrogen.

To fabricate  $\alpha$ -SiAlON/hBN composites, the tBN powders were mixed with other constituents ( $Y_2O_3$ ,  $\alpha$ - $Si_3N_4$ , AlN,  $\alpha$ -SiAlON seeds) and ball milled for 24 h. The mixture was dried and sifted through a 325-mesh sieve (45  $\mu$ m openings). Hot pressing was performed in a graphite furnace in nitrogen atmosphere (1 atm pressure) at a uniaxial pressure of 30 MPa. The heating rate was 15°C/min, followed by holding at 1900°C for 1 h and cooling in the furnace (approximately 50°C/min down to 1500°C). During initial heating, the chamber was evacuated and held for 1 h at 1000°C to remove absorbed organic residues from the powder surface, before the pressure was applied. For comparison, the same composites were fabricated using commercial hBN powders.

In an attempt to obtain a more uniform dispersion of BN and  $Si_3N_4$ , we also directly formed tBN onto  $Si_3N_4$  carrier particles as schematically described by the route on the right in Fig. 1. Melamine diborate precipitates were first mixed with  $\alpha$ - $Si_3N_4$  for 2 h (ball milling with 10 mm  $Si_3N_4$  balls in an anhydrous isopropanol liquid medium in a polyethylene jar). This was followed by drying in a rotary evaporator under vacuum, followed by holding in an oven at 70°C for 24 h, and then pyrolyzing under the same conditions as above. This  $Si_3N_4$ /BN mixture was also used to fabricate  $\alpha$ -SiAlON/hBN composite after mixing with other constituents and hot pressing in the same way as described above.

Phase composition was characterized by X-ray diffraction (XRD) analysis using a diffractometer with  $CuK\alpha$  radiation. IR spectra were acquired with a Perkin-Elmer FTIR System (Model 2000, Wellesley, MA). Microstructure characterization of sintered samples was performed on fractured or polished sections using a scanning electron microscope (SEM) JEOL-6400 and JEOL-6300 (Peabody, MA). The  $R$  curves of the hot-pressed materials were recorded by *in situ* observation of crack propagation in bars (30 mm  $\times$  2 mm  $\times$  3 mm) cut from the hot-pressed samples and loaded in four-point bending with an outer span of 20 mm and inner span of 10 mm.<sup>18</sup> The flexural strength was measured on bars (30 mm  $\times$  2 mm  $\times$  1.5 mm) with edges chamfered at 45° and tensile surfaces polished down to 1  $\mu$ m with diamond paste. Samples were loaded in three-point bending

with a span of 12.5 mm at a displacement rate of 0.2 mm/min. Estimate for the bending modulus was obtained from the same test using the linear portion of the load–displacement curve. Here the compliance of the crosshead and fixture was measured using the same setup but without the sample, and it was subtracted from the total compliance of the actual test with the sample. The procedure was calibrated using a monolithic  $\alpha$ -SiAlON sample assuming its Young's modulus was 300 GPa. Hardness testing was performed with a Shimadzu Vickers Hardness Tester (HSV-20), loaded at 10 kg for 10 s. Machinability of composites was evaluated by drilling a hole in a 4-mm-thick plate of ceramic with a spear-shaped carbide-tipped 1/8 inch drill bit. Roughness of the drilled surface was measured using a Dektak IIA (Veeco Inc., Woodbury, NY) profile measurement system on 1-mm line scans in the drilling direction.

### III. Results

#### (1) Formation of BN

Melamine diborate precipitates had needle-like crystal morphology with a length up to 100  $\mu$ m and a width of 1–5  $\mu$ m

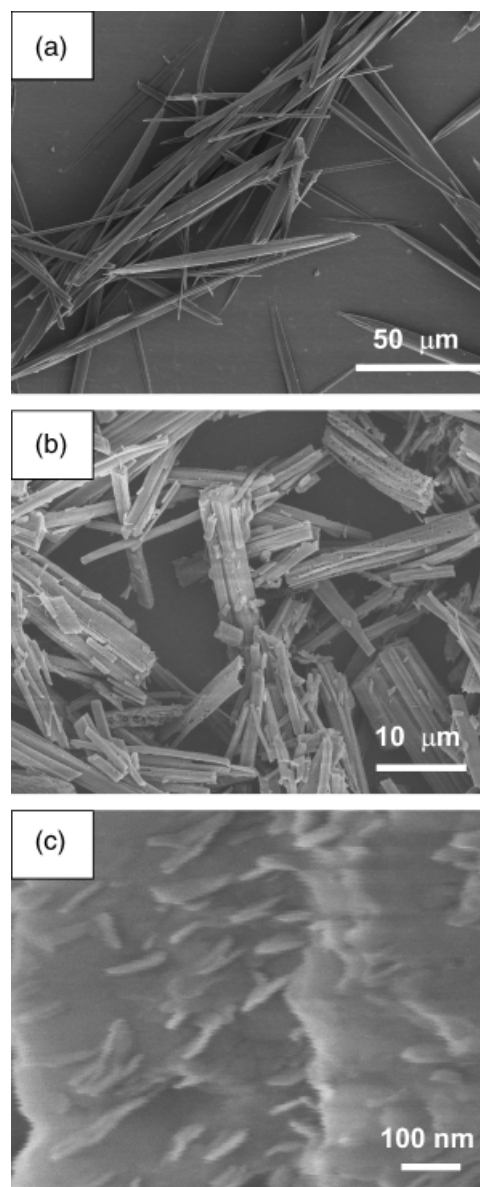
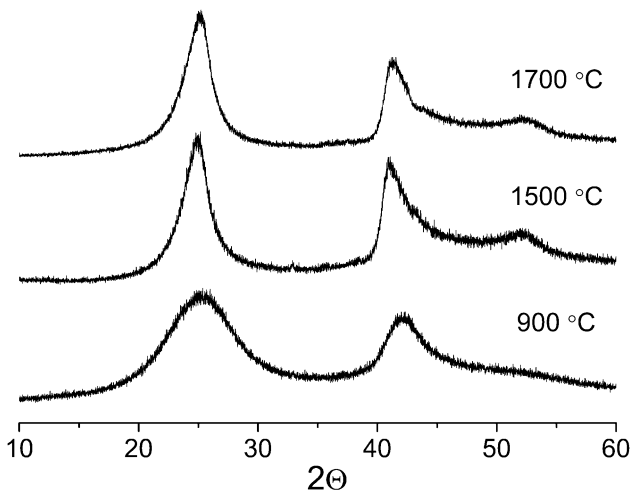


Fig. 2. Scanning electron micrographs of (a) as-precipitated  $C_3N_6H_6 \cdot 2H_3BO_3$  salt, used as a precursor for the preparation of turbostratic boron nitride (tBN), (b) tBN annealed at 1700°C, the bulk retaining the shape of (a), and (c), (b) at higher magnification showing individual 100-nm-sized tBN platelets.



**Fig. 3.** X-ray diffraction patterns of tBN prepared by firing to different temperatures: 900°C (20 h, NH<sub>3</sub>), 1500°C (20 h, NH<sub>3</sub>), and 1700°C (2 h in N<sub>2</sub>, after pyrolysis at 1500°C for 20 h in NH<sub>3</sub>).

(Fig. 2(a)). During pyrolysis, water vapor and CO<sub>2</sub> as reaction products were produced starting at ~600°C. After pyrolysis at 900°C the product was a white fluffy white powder that retained the shape of the precipitate except for some delamination within the needles. The mass yield was 100%–105% relative to the theoretical value expected for pyrolysis in NH<sub>3</sub>, meaning that the conversion was essentially complete. To proceed, the batches with a yield closest to the theoretical value (in the range 100%–102%) were selected for subsequent experiments. Pyrolysis at 1500°C followed by annealing at 1700°C retained the overall morphology of the precipitate crystals (Fig. 2(b)), but at higher magnification they revealed fine platelet-like particles with a diameter up to ~100 nm and a thickness of ~10 nm (Fig. 2(c)). At this stage the XRD pattern corresponded to that of tBN with a higher degree of crystallinity than achieved at 900°C (Fig. 3). FT-IR spectra (Fig. 4) presented further evidence for the formation of BN starting at 900°C, with features at 1360 and 810 cm<sup>-1</sup> that can be attributed to B–N stretching vibrations and N–B–N bending vibrations, respectively.<sup>12,19</sup> The impurity traces (marked with arrows in Fig. 4) in the 900°C product were very similar to those observed by Hagio *et al.*,<sup>15</sup> while the product at 1500° and 1700°C revealed only pure BN.

When melamine diborate precipitates were directly mixed with  $\alpha$ -Si<sub>3</sub>N<sub>4</sub> carrier powders (0.5  $\mu$ m mean particle size, see

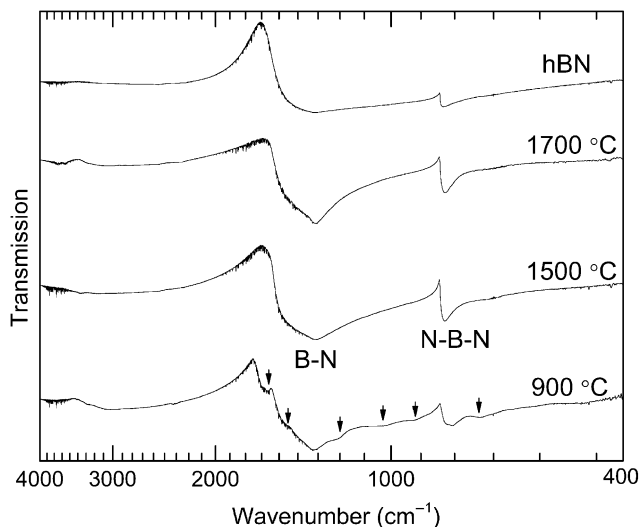


**Fig. 4.** FT-IR spectra of boron nitride (BN) prepared by pyrolysis to different temperatures same as in Fig. 3, compared with those of reference commercial hexagonal boron nitride (hBN) (top). Features attributed to impurities marked by arrows. (See text).

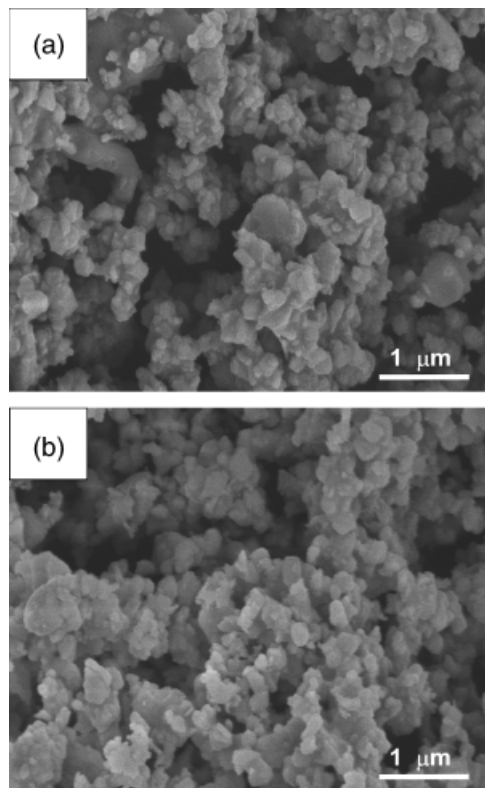


**Fig. 5.** Scanning electron micrographs of (a) as-received  $\alpha$ -Si<sub>3</sub>N<sub>4</sub> powder used as carrier particles for boron nitride (BN), and (b) BN-coated Si<sub>3</sub>N<sub>4</sub> powder (82 wt% Si<sub>3</sub>N<sub>4</sub>+18 wt% BN) after pyrolysis at 1500°C for 20 h in NH<sub>3</sub> followed by annealing at 1700°C for 2 h in N<sub>2</sub>.

Fig. 5(a)), after pyrolysis at either 900°C (not shown) or 1700°C (Fig. 5(b)) the powders maintained the same appearance. Neither did XRD reveal anything other than  $\alpha$ - and  $\beta$ -Si<sub>3</sub>N<sub>4</sub> (Fig. 6(a); a similar amount of  $\beta$ -Si<sub>3</sub>N<sub>4</sub> was also present in the as-received  $\alpha$ -Si<sub>3</sub>N<sub>4</sub> powders). Apparently, dispersion of BN precursor on Si<sub>3</sub>N<sub>4</sub> carrier particles made it difficult to form tBN with a sufficiently high crystallinity or large size to produce resolvable XRD reflections. It is also noted that hBN, the

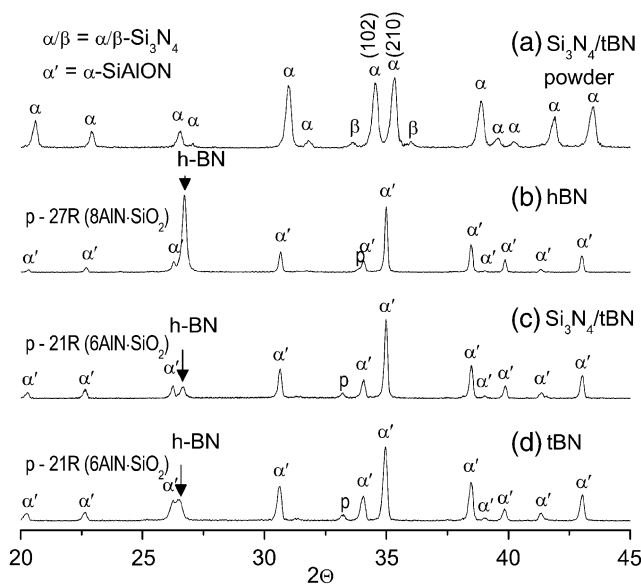


**Fig. 6.** X-ray diffraction patterns of (a) boron nitride (BN)-coated Si<sub>3</sub>N<sub>4</sub> powder same as in Fig. 5(b), showing peaks of  $\alpha$ - and  $\beta$ -Si<sub>3</sub>N<sub>4</sub> but not BN; and various  $\alpha$ -SiAlON/20BN composites prepared from (b) commercial hexagonal boron nitride (hBN), (c) Si<sub>3</sub>N<sub>4</sub>/turbostratic boron nitride (tBN) shown in (a), and (d) tBN. Both Si<sub>3</sub>N<sub>4</sub>/tBN and tBN were products of pyrolysis at 900°C.

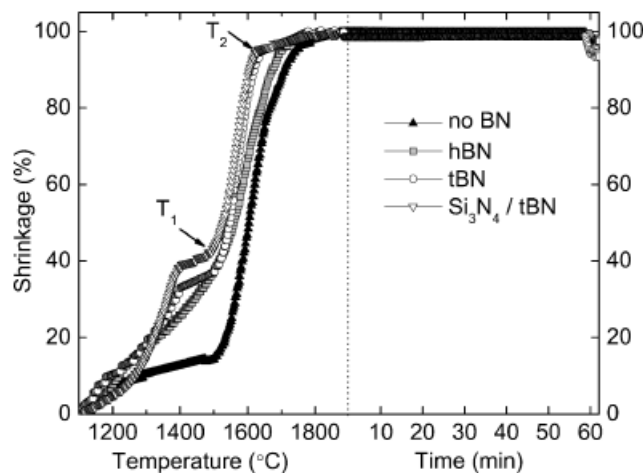


Fig. 7. Densification curves of  $\alpha$ -SiAlON (filled triangles) and  $\alpha$ -SiAlON/20 boron nitride (BN) composites. Sources for BN were commercial hexagonal boron nitride (hBN), turbostratic boron nitride (tBN), and  $\text{Si}_3\text{N}_4/\text{BN}$ , in the order of decreasing size.

thermodynamically stable phase, was not observed in any pyrolysis product, with or without  $\text{Si}_3\text{N}_4$ .

### (2) Microstructure of $\alpha$ -SiAlON/BN Composites

Densification curves of  $\alpha$ -SiAlON/20BN composites, regardless of the source of BN, all contained a pronounced low-temperature densification step that was absent in  $\alpha$ -SiAlON without additives (Fig. 7). This step was the least evident when using commercial hBN but was the most pronounced when using commercial hBN but was the most pronounced when using  $\text{Si}_3\text{N}_4/\text{tBN}$ . There was also a rapid densification stage (between  $T_1$  and  $T_2$  in Fig. 7), which has been attributed to nitride dissolution.<sup>20,21</sup> Here the starting temperature ( $T_1$ ) was relatively constant but the finishing temperature ( $T_2$ ) systematically decreased with increasing magnitude of the low-temperature step. The extra densification step was most likely related to BN dissolution, which was easier for smaller BN sizes, as in  $\text{Si}_3\text{N}_4/\text{tBN}$  where BN was well dispersed. XRD patterns of hot-pressed composites all showed hBN peaks (Figs. 6(b)–(d)). Apparently, although “dry”  $\alpha$ - $\text{Si}_3\text{N}_4$  and BN had no reaction with each other up to 1700°C (see Fig. 6(a) for 1700°C pyrolyzed  $\text{Si}_3\text{N}_4/\text{BN}$ ), once oxide sintering liquid was available at the initial stage of hot pressing, BN powders could dissolve and re-precipitate as hBN.

Analysis of XRD patterns and SEM micrographs indicated a further correlation between the size of the initial BN and the size of hBN in the composites, as well as the texture of both hBN and  $\alpha$ -SiAlON. As the X-ray scattering cross-section for BN was much lower than that of  $\alpha$ -SiAlON, the rather strong XRD intensity of the hBN (002) peak at  $\sim 27^\circ$  in the composites (Figs. 6(b)–(d)) was entirely a result of the hBN texture. It follows that the strongest hBN texture occurred when using hBN (Fig. 6(b)), and the weakest texture was obtained when using  $\text{Si}_3\text{N}_4/\text{tBN}$  (Fig. 6(c)). Meanwhile, the texture of  $\alpha$ -SiAlON, compared with that of monolithic  $\alpha$ -SiAlON, as illustrated by the peak height ratio of  $I(210)/I(102)$  shown in Fig. 8, was enhanced by BN addition when the hBN peak was strong.

The microstructures of  $\alpha$ -SiAlON/20BN using different BN powders are compared in Fig. 9. When hBN powders (diameter  $\sim 3$ – $5 \mu\text{m}$ ) were used (Fig. 9(a)), the length of the final intergranular BN grains, which have a flaky appearance, was several micrometers. In support of the XRD evidence of strong texture, these hBN grains were preferentially aligned in the plane perpendicular to the hot-pressing direction. These particles experienced some agglomeration, forming aggregates of up to  $\sim 10 \mu\text{m}$  in size. In contrast, when tBN (pyrolyzed at 900°C) or  $\text{Si}_3\text{N}_4/\text{tBN}$  (final annealing at 1700°C) was used, primarily submicron-

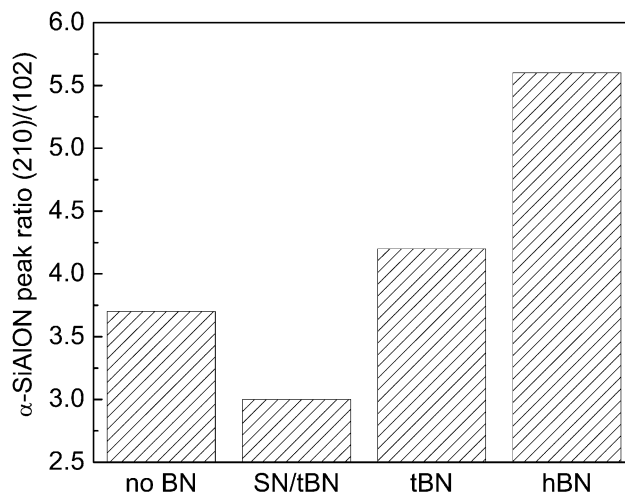


Fig. 8. X-ray diffraction peak height ratio of  $\alpha$ -SiAlON (210)/(102) in monolithic  $\alpha$ -SiAlON and  $\alpha$ -SiAlON/20BN composites same as in Fig. 7. Degree of texture increases with BN particle size.

sized hBN grains with agglomerates less than  $\sim 2 \mu\text{m}$  in diameter were seen, as shown in Figs. 9(b)–(c), respectively. These hBN grains had no apparent preferred orientation even though some  $\alpha$ -SiAlON texture was still evident. Meanwhile, compared with that of the  $\alpha$ -SiAlON monolith (Fig. 9(d)), the size and aspect ratio of elongated  $\alpha$ -SiAlON grains were reduced, as shown in Figs. 9(b)–(c). The homogeneous distribution of sub-micron-sized hBN grains was also confirmed by backscattered-electron (BE) SEM images as, for example, for the composite that used tBN pyrolyzed at 900°C (Fig. 10). This micrograph further established that the amount of residual grain boundary phase, which appears white in Fig. 10 because of a higher Y content, was quite small despite BN addition. Lastly, the grain size of hBN was essentially independent of the BN amount in the range from 5 to 40 vol% (not shown).

### (3) Mechanical Properties of $\alpha$ -SiAlON/BN Composites

The mechanical properties of these composites followed systematic trends. For conciseness, we will focus on comparing samples made from commercial hBN powders and those from 900°C pyrolyzed tBN powders, for which we have most extensive data.

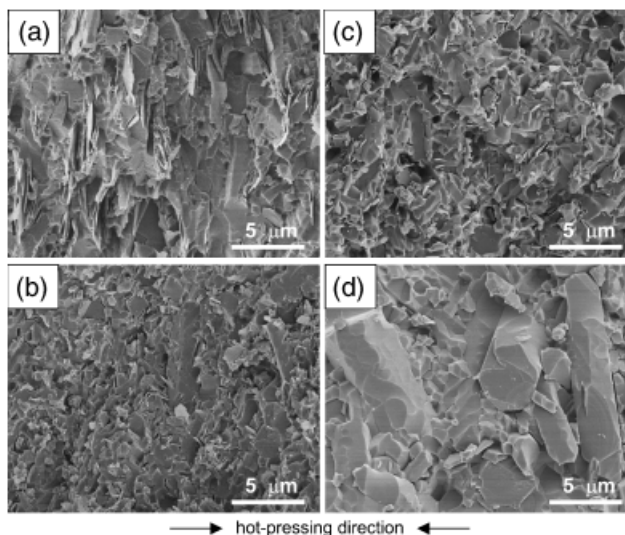
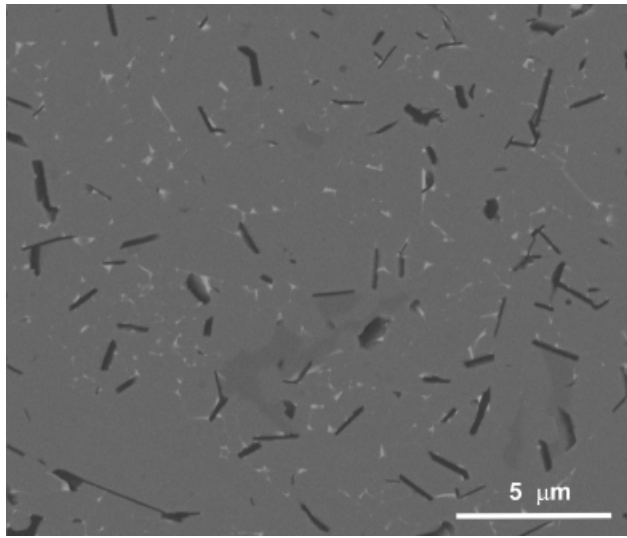


Fig. 9. Scanning electron micrographs of  $\alpha$ -SiAlO/20BN composites prepared from (a) commercial hexagonal boron nitride (hBN), (b) turbostratic boron nitride (tBN) (pyrolyzed at 900°C), and (c)  $\text{Si}_3\text{N}_4/\text{BN}$  (annealed at 1700°C), compared with (d)  $\alpha$ -SiAlON monolith.



**Fig. 10.** Backscattered-electron scanning electron microscope (BE SEM) image of polished surface of  $\alpha$ -SiAlON/20BN composite prepared from turbostratic boron nitride (tBN) (pyrolyzed at 900°C). Dark areas: BN platelets (average diameter <2  $\mu\text{m}$ ). White areas: grain boundary phase.

The 5BN composites were not machinable, and the 10BN composites chipped during drilling. The 20BN composites could be machined easily (Fig. 11) regardless of the source of BN, although some edge chipping was occasionally observed in those made from commercial hBN powders. This correlates with the increasing number of intergranular BN particles in composites with higher BN contents (not shown). The surface roughness of the “nanocomposite” (from  $\text{Si}_3\text{N}_4$ /tBN precursor) was only half of that of the microcomposite from commercial hBN (see Table II). The drill groove was continuous and apparent in the nanocomposite and less so in the microcomposite because of the track-breakdown caused by the surface damage (Fig. 12). These observations are in good accord with those reported in Kusunose *et al.*<sup>2</sup>

The hardness of the composites decreased with increasing BN content; however, composites with a finer microstructure were harder, with the 20BN composites made from tBN being almost twice as hard as those made from commercial hBN (Fig. 13). A size effect was also manifested in the room-temperature flexural strength of the 20BN composites, being  $811 \pm 30$  MPa for the one made from tBN,  $806 \pm 40$  MPa for the one made from  $\text{Si}_3\text{N}_4$ /tBN (both pyrolyzed at 900°C), and  $535 \pm 15$  MPa for the one made from commercial hBN. Comparing these values with the strength of  $\sim 940$  MPa of  $\alpha$ -SiAlON monolith without BN, it becomes apparent that a homogeneous addition of fine BN particles to  $\alpha$ -SiAlON is not detrimental to the strength despite its softening effect on elastic (bending) modulus (Fig. 13). Indeed, the strength retention of the composites with fine BN was the same as that of monolithic  $\alpha$ -SiAlON up to 1000°C, above which the composite strength decreased rapidly, which was

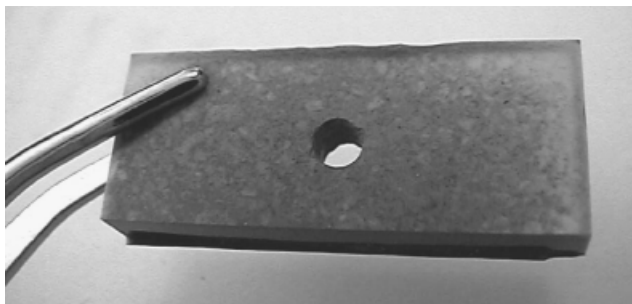


**Fig. 11.** Hole drilled in  $\alpha$ -SiAlON/20BN composite (prepared from  $\text{Si}_3\text{N}_4$ /turbostratic boron nitride (tBN)), demonstrating machinability.

**Table II.** Mean Roughness ( $R_a$ ) and Maximum Roughness ( $R_{\text{max}}$ ) of the Drilled Surface in the Microcomposite (from hBN) and Nanocomposite (from  $\text{Si}_3\text{N}_4$ /tBN, Pyrolyzed at 900°C)

Roughness	Microcomposite	Nanocomposite
$R_a$ ( $\mu\text{m}$ )	0.61	0.35
$R_{\text{max}}$ ( $\mu\text{m}$ )	6.09	2.78

tBN, turbostratic boron nitride; hBN, hexagonal boron nitride.

accompanied by a similar decrease of elastic modulus (Fig. 14). The fracture resistance of the composites was considerably lower than that of  $\alpha$ -SiAlON and exhibited a rather flat  $R$  curve (Fig. 15).

#### IV. Discussion

The melamine–diborate process proved to be more suitable than the boric acid/urea process for preparing tBN, showing no sign of precursor melting during pyrolysis. Indeed, even after annealing at 1700°C, the shape of salt crystals was preserved by BN bundles (Fig. 2(b)), in agreement with similar reports in the literature.<sup>14,15</sup> The product tBN was of good purity, with a mass yield close to 100% and low impurity content according to IR spectra. Although the variable interlayer distances of tBN make it impossible to determine the crystallite size from XRD, SEM micrographs showed that each BN bundle was a collection of flake-like fine crystals  $\sim 100$  nm in diameter (Fig. 2(c)). These bundles are likely to break up into finer crystallites during milling in composite fabrication. For the  $\text{Si}_3\text{N}_4$ /BN powders, the BN size is probably even smaller as XRD could not detect tBN after pyrolysis (Fig. 6(a)), in agreement with Hojo *et al.*<sup>22</sup> It was reported in other studies that under similar annealing conditions, but using urea and boric acid, carrier particles were coated

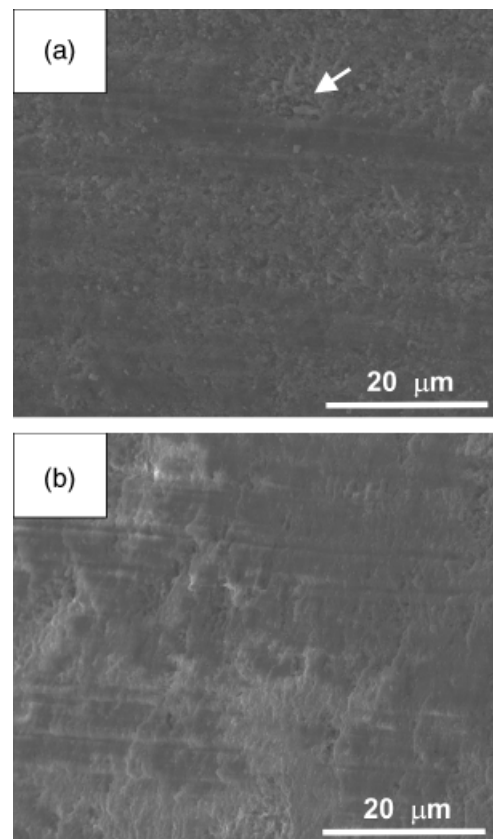


**Fig. 12.** Scanning electron micrographs of drilled hole surfaces in (a) microcomposite and (b) nanocomposite (prepared from  $\text{Si}_3\text{N}_4$ /turbostratic boron nitride (tBN) pyrolyzed at 900°C). Arrow points to a chip in microcomposite.

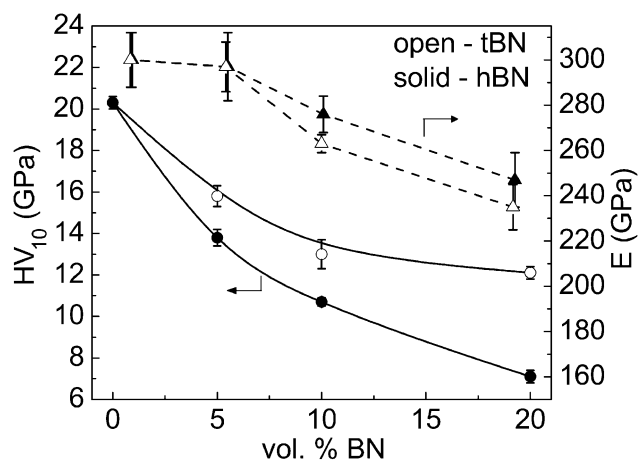


Fig. 13. Hardness and elastic (bending) modulus of  $\alpha$ -SiAlON/ $x$ BN, prepared using turbostratic boron nitride (tBN) pyrolyzed at 900°C (open symbols) or hexagonal boron nitride (hBN) (solid symbols).

with hBN films of a thickness of several nanometers.<sup>1,10,19,23,24</sup> This thickness is below the resolution of the SEM we used, and it also would not have resulted in any resolvable XRD peak of BN. However, although the melamine-diborate process can lead to a homogeneous mixture of very fine BN particles and other powders, BN nevertheless dissolves and then re-precipitates during liquid phase sintering. Therefore, the final size of hBN in the composites is considerably coarser, of the order of 1  $\mu$ m. At this point, it is not clear whether BN from any precursor processing routes can avoid solution/reprecipitation, yet undergo turbostratic to hexagonal phase transformation, during liquid phase sintering.

Although BN coarsens during liquid phase sintering, its presence apparently provides Zener pinning<sup>1,25,26</sup> that inhibits the growth of  $\alpha$ -SiAlON grains. As the pinning effect is stronger the smaller the size of BN, it explains the different microstructures in Fig. 9. In addition, as the hot-pressing texture typically increases with the size of elongated grains, an associated BN size effect on composite texture also results (Fig. 8). Similar texture observations on  $\beta$ -Si<sub>3</sub>N<sub>4</sub> grains in  $\beta$ -Si<sub>3</sub>N<sub>4</sub>/BN composites were reported by Kusunose *et al.*<sup>1</sup> Grain growth inhibition by BN was also observed by Zhang and Ohji<sup>6</sup> on SiC/BN and  $\beta$ -Si<sub>3</sub>N<sub>4</sub>/SiC/BN composites,<sup>27</sup> and by Kusunose *et al.*<sup>1</sup> on  $\beta$ -Si<sub>3</sub>N<sub>4</sub>-BN composites.

The mechanical properties of our composites manifest another BN size effect: the smaller the BN particles, the higher the strength and hardness. Note that hBN platelet in the

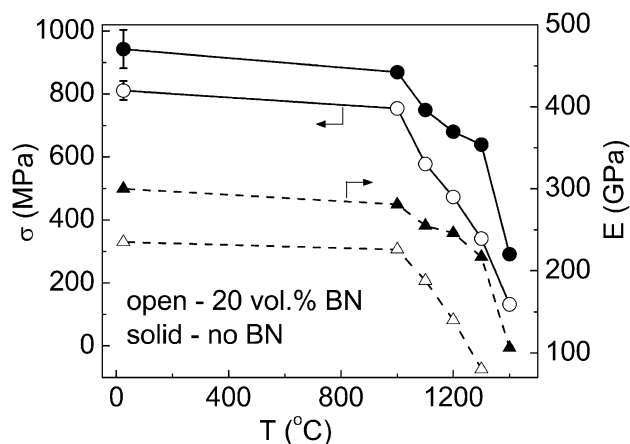


Fig. 14. Temperature dependence of strength and elastic (bending) modulus of  $\alpha$ -SiAlON (solid symbols) and  $\alpha$ -SiAlON/20BN composite (open symbols), prepared using turbostratic boron nitride (tBN; pyrolyzed at 900°C), with similar strength and modulus retention at 1000°C.

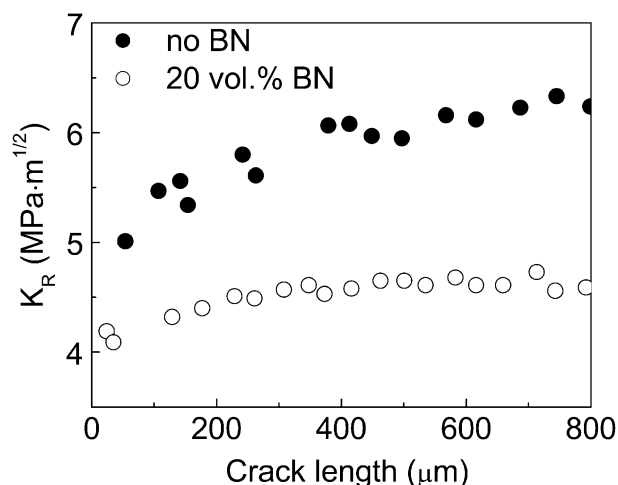


Fig. 15.  $R$  Curves of  $\alpha$ -SiAlON and  $\alpha$ -SiAlON/20BN composite, prepared from turbostratic boron nitride (tBN; pyrolyzed at 900°C).

composites has low elastic modulus, low hardness, and an anisotropic thermal expansion coefficient. (For hBN,  $E = 43$  MPa,  $\alpha = 0.57 \times 10^{-6} \text{K}^{-1}$  parallel to  $c$ -axis,  $-0.46 \times 10^{-6} \text{K}^{-1}$  perpendicular to  $c$ -axis, hardness = 1.5 on the Mohs scale and easy cleavage along the basal plane.)<sup>28</sup> During cooling hBN flakes cleave easily perpendicular to the  $c$ -axis, forming microcracking, as shown by Zhang *et al.*<sup>27</sup> Microcracks can also form at the interface between BN and the matrix. Size effect of BN particles is related to the stress concentration around an elastically compliant inclusion or microcrack. Thus, composite fracture is controlled by the largest flaw size, which is probably correlated to the size of the hBN platelet. The size effect on hardness may be due to a similar reason, in that hBN platelet acts as an elastically and plastically soft inclusion, causing a shear-stress concentration that induces plastic deformation nearby. This stress concentration also depends on the size of the platelet, and hence larger hBN platelets have a larger softening effect on the composite hardness.

On the other hand, the weakening effect of second-phase platelets on the elastic modulus of a composite is size independent; instead, it scales with the product of aspect ratio and the volume fraction of the platelets or microcracks.<sup>29,30</sup> The lack of a size effect is consistent with our results in that the composite moduli are independent of the source of BN, which have different diameters (Fig. 13). However, the modest modulus reduction, about 20% in 20BN composites at room temperature, is smaller than expected for those hBN platelets studied here, which have an aspect ratio considerably greater than one. This is probably because, in bending, tensile and compressive stresses on the two sides of the neutral axis are balanced, but only the tensile side experiences a weakening effect of the microcracks, whereas on the compressive side the shut cracks are still load bearing. Therefore, only 50% of the hBN platelets contribute to elastic weakening, and hence only a modest modulus reduction results.

Lastly, our observation of good machinability, high strength, and lower, flatter  $R$  curve of the composites strongly suggests that these properties are not directly correlated to each other. As already mentioned, strength is controlled by the largest flaw size. Therefore, high strength can still be achieved even if the composite contains many weak inclusions, provided the inclusions are small enough. It is also well known that the toughening effect (including rising  $R$  curve) due to second-phase bridging and pullout decreases with the particle size.<sup>31</sup> This, along with Zener pinning that reduces the grain size of the matrix, explains the low toughness of the composites that contain very small hBN platelets. On the other hand, improved machinability is attributed to the weak interface afforded by hBN platelets, allowing grain detachment and quasi-plastic deformation under machining

stresses. We may therefore expect that the size of the machining chips formed is commensurate with the spacing between hBN platelets, and that a small chip size in turn prevents the formation of critical machining flaws that can cause premature fracture. With hBN platelets of the same size, an increase in hBN content should decrease the chip size and lead to better machinability.<sup>2</sup> This is consistent with the microstructure observed in our study, in which the hBN size appeared relatively constant regardless of the BN volume fraction.

## V. Conclusions

Nanosized tBN powder can be prepared by pyrolysis of melamine diborate salt in ammonia gas. Similarly,  $\alpha$ -Si<sub>3</sub>N<sub>4</sub> powders coated with BN can be obtained when carrier  $\alpha$ -Si<sub>3</sub>N<sub>4</sub> powders are mixed with melamine diborate before pyrolysis.

Using nanosized tBN or BN-coated Si<sub>3</sub>N<sub>4</sub> powders,  $\alpha$ -SiAlON/BN composites with homogeneously distributed micron-sized hBN platelets have been obtained. In contrast, composites produced from commercial coarse-grained hBN powders contained much larger hBN platelets with an overall coarser microstructure.

The size and distribution of the hBN platelets were found to be the determining factors for the mechanical properties of the composites. Coarse hBN platelets cause significant strength and hardness degradation, whereas composites with fine hBN platelets have strength close to that of monolithic  $\alpha$ -SiAlON. Composites with 20 vol% of fine hBN are machinable despite a flat *R* curve.

## References

- <sup>1</sup>T. Kusunose, T. Sekino, Y. H. Choa, and K. Niihara, "Fabrication and Microstructure of Silicon Nitride/Boron Nitride Nanocomposites," *J. Am. Ceram. Soc.*, **85** [11] 2678–8 (2002).
- <sup>2</sup>T. Kusunose, T. Sekino, Y.-H. Choa, and K. Niihara, "Machinability of Silicon Nitride/Boron Nitride Nanocomposites," *J. Am. Ceram. Soc.*, **85** [11] 2689–95 (2002).
- <sup>3</sup>T. Kusunose, Y.-H. Choa, T. Sekino, and K. Niihara, "Mechanical Properties of Si<sub>3</sub>N<sub>4</sub>/BN Composites by Chemical Processing," *Key Eng. Mater.*, **161–163**, 475–9 (1999).
- <sup>4</sup>T. Kusunose, R.-J. Sung, T. Sekino, S. Sakaguchi, and K. Niihara, "High-Temperature Properties of a Silicon Nitride/Boron Nitride Nanocomposite," *J. Mater. Res.*, **19** [5] 1432–8 (1994).
- <sup>5</sup>G.-J. Zhang, J.-F. Yang, T. Ohji, and S. Kanzaki, "In-Situ Reaction Synthesis of Non-Oxide Boron Nitride Composites," *Adv. Eng. Mater.*, **4** [1–2] 15–7 (2002).
- <sup>6</sup>G.-J. Zhang and T. Ohji, "Effect of BN Content on Elastic Modulus and Bending Strength of SiC–BN *In Situ* Composites," *J. Mater. Res.*, **15** [9] 1876–80 (2000).
- <sup>7</sup>G.-J. Zhang, J.-F. Yang, M. Ando, and T. Ohji, "SiAlON–Boron Nitride Porous Composites: *In Situ* Synthesis, Microstructure and Properties," *Key Eng. Mater.*, **237**, 123–8 (2003).

- <sup>8</sup>Y. Uemura, S. Nisimura, T. Sato, and M. Tansho, "BN–Si<sub>3</sub>N<sub>4</sub> Composite Synthesized by Direct Nitridation of SiB<sub>6</sub> Alloy," *Key Eng. Mater.*, **206** [2] 1137–40 (2002).
- <sup>9</sup>W. S. Coblenz and D. Lewis III, "*In Situ* Reaction of B<sub>2</sub>O<sub>3</sub> with AlN and/or Si<sub>3</sub>N<sub>4</sub> to Form BN-Toughened Composites," *J. Am. Ceram. Soc.*, **71** [12] 1080–5 (1988).
- <sup>10</sup>T. Oku, T. Kusunose, T. Hirata, N. Sato, R. Hatakeyama, K. Niihara, and K. Suganuma, "Formation and Structure of Ag, Ge and SiC Nanoparticles Encapsulated in Boron Nitride and Carbon Nanocapsules," *Diamond Relat. Mater.*, **9** [3–6] 911–5 (2000).
- <sup>11</sup>O. Yamamoto, "Crystalline Turbostratic Boron Nitride Powder and Method for Producing Same"; U.S. Patent No. 6,306,358, October 23, 2001.
- <sup>12</sup>M. Hubacek, T. Sato, and T. Ishii, "A Coexistence of Boron Nitride and Boric Acid," *J. Solid State Chem.*, **109**, 384–90 (1994).
- <sup>13</sup>K. Koeda and C. Ito, "Process for Producing Boron Nitride"; U.S. Patent No. 4,562,050, December 31, 1985.
- <sup>14</sup>F. Fauzi, M. Tani, and M. Suzue, Boron Nitride and Process for Preparing the Same U.S. Patent No. 6,319,602, November 20, 2001.
- <sup>15</sup>T. Hagio, K. Kobayashi, and T. Sato, "Formation of Hexagonal BN by Thermal Decomposition of Melamine Diborate," *J. Ceram. Soc. Jpn.*, **102** [11] 1051–4 (1994).
- <sup>16</sup>M. Zenotchkine, R. Shuba, J. S. Kim, and I. W. Chen, "Synthesis of  $\alpha$ -SiAlON Seed Crystals," *J. Am. Ceram. Soc.*, **84** [7] 1651–3 (2001).
- <sup>17</sup>M. Zenotchkine, R. Shuba, and I.-W. Chen, "Liquid-Phase Growth of Small Crystals for Seeding Alpha-SiAlON Ceramics," *J. Am. Ceram. Soc.*, **87** [6] 1040–6 (2004).
- <sup>18</sup>M. Zenotchkine, R. Shuba, J. S. Kim, and I.-W. Chen, "R-Curve Behavior of *In Situ* Toughened—SiAlON Ceramics," *J. Am. Ceram. Soc.*, **84** [4] 884–6 (2001).
- <sup>19</sup>D.-F. Lii, J.-L. Huang, L.-J. Tsui, and S.-M. Lee, "Formation of BN Films on Carbon Fibers by Dip-Coating," *Surf. Coat. Technol.*, **150** [2–3] 269–76 (2000).
- <sup>20</sup>M. Menon and I. W. Chen, "Reaction Densification of  $\alpha$ -SiAlON: I. Wetting Behavior and Acid–Base Reactions," *J. Am. Ceram. Soc.*, **78** [3] 545–52 (1995).
- <sup>21</sup>M. Menon and I. W. Chen, "Reaction Densification of  $\alpha$ -SiAlON II. Densification Behavior," *J. Am. Ceram. Soc.*, **78** [3] 553–9 (1995).
- <sup>22</sup>J. Hojo, K. Eto, M. Uehara, and N. Enomoto, "Spectroscopic Evaluation of Nanocomposite Formation from Amorphous Complex Compound in Si<sub>3</sub>N<sub>4</sub>–BN System," *Scripta Mater.*, **44** [8–9] 2169–72 (2001).
- <sup>23</sup>J. Li and L. Gao, "Preparation of h-BN Nano-Film Coated  $\alpha$ -Si<sub>3</sub>N<sub>4</sub> Composite Particles by a Chemical Route," *J. Mater. Chem.*, **13** [3] 628–30 (2003).
- <sup>24</sup>T. Masui, M. Yamamoto, T. Sakata, H. Mori, and G.-Y. Adachi, "Synthesis of BN-Coated CeO<sub>2</sub> Fine Powder as a New UV Blocking Material," *J. Mater. Chem.*, **10** [2] 384–90 (2000).
- <sup>25</sup>L. A. Xue, K. Meyer, and I. W. Chen, "Control of Grain-Boundary Pinning in Al<sub>2</sub>O<sub>3</sub>/ZrO<sub>2</sub> Composites With Ce<sup>3+</sup>/Ce<sup>4+</sup> Doping," *J. Am. Ceram. Soc.*, **75** [4] 822–9 (1992).
- <sup>26</sup>L. C. Stearns and M. P. Harmer, "Particle-Inhibited Grain Growth in Al<sub>2</sub>O<sub>3</sub>–SiC: II, Equilibrium and Kinetic Analyses," *J. Am. Ceram. Soc.*, **79** [12] 3020–8 (1996).
- <sup>27</sup>G. J. Zhang, J. F. Yang, and T. Ohji, "*In situ* Si<sub>3</sub>N<sub>4</sub>–SiC–BN Composites: Preparation, Microstructures and Properties," *Mater. Sci. Eng. A*, **328** [1–2] 201–5 (2002).
- <sup>28</sup>C. A. Harper (ed.) *Handbook of Materials for Product Design*. McGraw-Hill, New York, 2001.
- <sup>29</sup>J. D. Eshelby, "The Determination of the Elastic Field of an Ellipsoidal Inclusion, and Related Problems," *Proc. Roy. Soc. London*, **A241**, 376–9 (1957).
- <sup>30</sup>I.-W. Chen and A. S. Argon, "Grain Boundary and Interphase Boundary Sliding in Power Law Creep," *Acta Metall.*, **27**, 749–54 (1979).
- <sup>31</sup>M. Zenotchkine, R. Shuba, and I.-W. Chen, "Effect of Seeding on the Microstructure and Mechanical Properties of  $\alpha$ -SiAlON: III, Comparison of Modifying Cations," *J. Am. Ceram. Soc.*, **86** [7] 1168–75 (2003). □